UNIVERSITY OF BIRMINGHAM

Particle Swarm Optimization for Optimal Frequency Response with High Penetration of Photovoltaic and Wind Generation

Alvarez-Alvarado, Manuel S.; Rengifo, Johnny; Gallegos-Núñez, Rommel M.; Rivera-Mora, José G.; Noriega, Holguer H.; Velasquez, Washington; Donaldson, Daniel; Rodríguez-Gallegos, Carlos D.

Document Version
Publisher's PDF, also known as Version of record

Link to publication on Research at Birmingham portal

Particle Swarm Optimization for Optimal Frequency Response with High Penetration of Photovoltaic and Wind Generation

Manuel S. Alvarez-Alvarado [1,*]**, Johnny Rengifo** [1]**, Rommel M. Gallegos-Núñez** [1]**, José G. Rivera-Mora** [1]**, Holguer H. Noriega** [1]**, Washington Velasquez** [1]**, Daniel L. Donaldson** [2] **and Carlos D. Rodríguez-Gallegos** [3]

[1] Escuela Superior Politécnica del Litoral (ESPOL), Guayaquil EC090112, Ecuador
[2] Department of Electronic, Electrical and Systems Engineering, University of Birmingham, Birmingham B15 2TT, UK
[3] Solar Energy Research Institute of Singapore (SERIS), National University of Singapore (NUS), Singapore 117574, Singapore
[*] Correspondence: mansalva@espol.edu.ec

Abstract: As the installation of solar-photovoltaic and wind-generation systems continue to grow, the location must be strategically selected to maintain a reliable grid. However, such strategies are commonly subject to system adequacy constraints, while system security constraints (e.g., frequency stability, voltage limits) are vaguely explored. This may lead to inaccuracies in the optimal placement of the renewables, and thus maximum benefits may not be achieved. In this context, this paper proposes an optimization-based mathematical framework to design a robust distributed generation system, able to keep system stability in a desired range under system perturbance. The optimum placement of wind and solar renewable energies that minimizes the impact on system stability in terms of the standard frequency deviation is obtained through particle swarm optimization, which is developed in Python and executed in PowerFactory-DIgSILENT. The results reveal that the proposed approach has the potential to reduce the influence of disturbances, enhancing critical clearance time before frequency collapse and supporting secure power system operation.

Keywords: particle swarm optimization; PV system; power system stability; optimization wind generation

1. Introduction

The incorporation of renewable energy sources (RES) into power systems has enabled meaningful changes to the structure of the grid, control techniques, and normal operation [1]. Thus, there are many important aspects to be considered by the system operators. The first aspect concerns the cost/benefit analysis associated with the application of PV and wind energy that must consider comprehensive system reliability assessment [2]. Another aspect is the availability of RES technology, i.e., there is a dependence of RES on weather conditions. For instance, a very extreme case occurs when a voltage collapse in a system with high penetration of photovoltaic (PV) generation, due to partial clouding [3]. Flexibility is another aspect to consider, and it denotes the ability of the system components to adjust their operating point, in a timely and harmonized manner, to accommodate expected, as well as unexpected, changes in system operating conditions [4,5]. In general, power system flexibility is a basic prerequisite for allowing higher RES penetration. Finally, but not less importantly, the stability of the power system is another topic to be taken into account when assessing the integration of RES [6–8], which is within the scope of this paper.

The implementation of distributed generation (DG) provides a reduction in power losses [9,10] and high system reliability [11,12]. Despite the many benefits from the implementation of DGs, surveys have suggested new challenges concerning the optimum location and size of them [13–15], i.e., an inadequate determination of DG location and size

may lead to an increase in system losses or even in system instability in short-circuit scenarios [16]. In this context, the literature proposes the incorporation of optimization methods into the power system stability analysis. For instance, [17] presents an improved equilibrium optimization algorithm (IEOA) combined with a recycling strategy for configuring the power distribution networks with optimal allocation of multiple distributed generators. A similar study can be found in [18], where the optimum DG placement and sizing are obtained through the incorporation of a novel stability metric known as power stability index (PSI). Another example is presented in [19], where the researchers propose a hybrid optimization to determine the optimal allocation of DG in the standard IEEE 33-bus radial distribution system in order to improve the voltage stability and minimize the total power loss. The proposed hybrid technique is based on the gray wolf optimization algorithm with a loss sensitivity factor. Even though these studies provide insightful methodologies for maximum system stability, these are limited to small signal stability analysis. Moreover, the impact on critical clearance time before frequency collapse is not clearly identified.

Given the above, this paper contributes to the state of the art with a particle swarm optimization (PSO) algorithm to minimize the impact of system perturbance on frequency response through the optimal size and location of various generation resources. The novelty of this work is the incorporation of a power system security indicator as an objective function to determine the allocation and size of renewable energies within a power system. The analysis considers a sudden and significant imbalance power between generation and load that leads to a frequency deviation. The results are assessed using dynamic indicators that quantify transient network disturbances, e.g., standard deviation frequency metric (SDF) and rate of change of frequency index (ROCOF). In addition, the critical clearance time (CCT) [20] is explored for a three-phase short-circuit fault in the power system, showing a significant enhancement when the renewable generator is placed in the optimum location. For this purpose, the rest of the paper is structured as follows: Section 2 describes the mathematical model of every component used in the transmission system, including the control system; Section 3 presents the optimization problem formulated by the objective function and constraints; Section 4 describes the algorithm used to solve the optimization problem; Section 5 gives details concerning the case study, which includes the transmission system used to validate the proposed approach; Section 6 presents a deep analysis of the results; finally, Section 7 provides the conclusions.

2. Mathematical Model

The power system includes PV systems, wind generators (WGs), synchronous generators, transformers, and loads. In order to formulate the PV system and WG optimal allocation as an optimization problem, it is required to define their mathematical model, including the control system. This is given below.

2.1. Photovoltaic System (PV)

Every single PV system presents an instantaneous output power $P_{solar}(t)$ obtained from the solar radiation [21] as follows:

$$P_{solar}(t) = A\eta_{PV}I(t) \tag{1}$$

where I is the solar radiation given in kW/m^2, A denotes the PV area, and η_{PV} is the overall efficiency of PV panels and DC-AC inverter. Considering N_{PV} as the number of PV systems, the overall produced power at any time t is given by Equation (2):

$$P_{PV}(t) = N_{PV} \, P_{solar}(t) \tag{2}$$

2.2. Wind Generation (WG)

The wind speed v is the key factor for WG. The generation starts when the wind speed exceeds the cut-in value v_{ci}. On the other hand, for mechanical protection purposes, the WG cannot provide power if the wind speed exceeds the cut-out value v_{co}. Another

scenario to consider is when the wind speed is between the wind speed rate v_r of the WG and the cut-out value, in which the injected power belongs to the rate power P_R of the WG. Finally, if the wind speed is between v_{ci} and v_r the power injected by each WG $P_{WG}(t)$ follows the mathematical expression as presented in Equation (3) [22].

$$P_{WG}(t) = \begin{cases} 0 & , \quad v(t) \leq v_{ci} \\ P_R \frac{v(t) - v_{ci}}{v_r - v_{ci}} & , \quad v_{ci} < v(t) < v_r \\ P_R & , \quad v_r \leq v(t) \leq v_{ci} \end{cases} \tag{3}$$

Similarly, as with the PV systems, let us consider N_{WT} as the total number of wind turbines; therefore, the overall produced power through time is

$$P_{WT}(t) = N_{WT} P_{WG}(t) \tag{4}$$

2.3. Load Frequency Control (LFC)

For stable operation of the system generation, the LFC manages the governor for speed regulation according to load variation. The LFC acts as a comparator, whose output ΔP_g is the difference between the set reference power ΔP_{ref} and the power $\Delta\omega/R$ given from the governor speed characteristics, which is described in the frequency domain, as shown in Equation (5).

$$\Delta P_g(s) = \Delta P_{ref}(s) - \frac{1}{R}\Delta\omega(s) \tag{5}$$

It should be considered that ΔP_g is transformed through the hydraulic amplifier into the valve position command of the work-performing source (e.g., steam) ΔP_V. Assuming a linear relationship and considering a simple time constant τ_g, the relationship ΔP_V can be described as a function of ΔP_g, as shown in Equation (6).

$$\Delta P_V(s) = \frac{1}{\tau_g s + 1}\Delta P_g(s) \tag{6}$$

The source of mechanical energy is attributed to the prime mover, which is associated with the turbine of the system. The model relates the changes in the mechanical power output ΔP_m to the changes in the valve position of the source that produces the work ΔP_V. The simplest prime mover model can be approximated using a time constant τ_t, which results in the transfer function shown in Equation (7).

$$\Delta P_m(s) = \frac{1}{\tau_T s + 1}\Delta P_V(s) \tag{7}$$

In addition, by considering the generator-load couple model based on inertial constant H and damping constant D of the generator, and by joining the governor and prime mover, the complete model of the LFC used in this paper is as presented in Figure 1 [23].
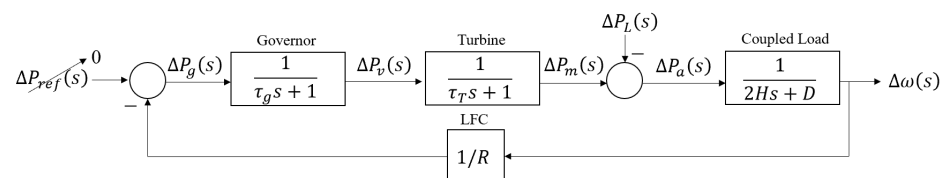
Figure 1. LFC block diagram.

2.4. Automatic Voltage Regulator with Power System Stabilization

Power system stabilization (PSS) is an important component of the control system for a synchronous generator which works as a feedback controller, across the excitation system, building up a signal to modulate the field voltage. Its main function is to damp generator rotor oscillations around electromechanical oscillations [24]. Figure 2 shows the control

block diagram of the PSS used in this manuscript [25]. The outcome of PSS is limited by a maximum and minimum range:
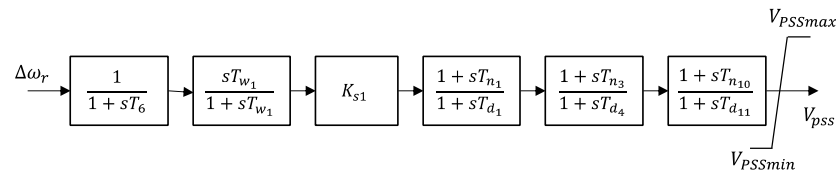
$$V_{PSSmin} \leq V_{PSS} \leq V_{PSSmax} \tag{8}$$

Figure 2. PSS block diagram.

On the other hand, the role of automatic voltage regulator (AVR) in a power system is to control the terminal voltage magnitude of a synchronous alternator according to a reference set point. A basic AVR system has four main components: sensor, amplifier, exciter, and generator [24]. The terminal generator voltage is endlessly measured by a voltage sensor. Later, the wave is rectified, smoothed, and contrasted with a reference set point. The error signal generated in the comparator is magnified and is utilized for the field winding controls of the generator. Figure 3 shows the transfer function with PSS controller used in this manuscript.
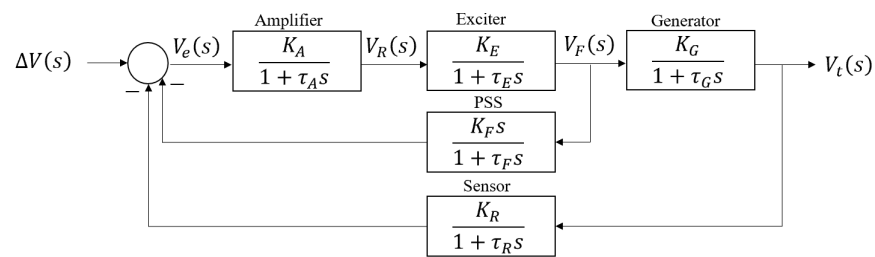

Figure 3. AVR block diagram.

3. Problem Formulation

The stability indices used in this paper are the SDF and ROCOF. The SDF index measures the variation of the steady-state frequency f_{ss} with respect to the instantaneous frequency f at any time t during a period equal to T, which mathematically is determined by Equation (9) [26]. This index is used as a metric to quantify the power system stability frequency response, such that an SDF value that is nearest to zero implies a better frequency response. On the other hand, the ROCOF focuses on measuring the control system robustness, such that a ROCOF value that is nearest to zero implies a better control response. This metric quantifies the frequency response rate just after an imbalance of power in the electrical power system (i.e., disconnection of a generator/load tripping), before the action of any control at time τ. Mathematically, the ROCOF can be expressed in terms of the power imbalance $\Delta P_{imbalance}$, power demanded P_{load}, frequency before the disturbance f_0, and inertia constant H, as presented in Equation (10) [27].

$$\text{SDF} = \sqrt{\frac{1}{T} \sum_{t=1}^{T} (f_t - f_{ss})^2} \tag{9}$$

$$\text{ROCOF} = \left. \frac{df}{dt} \right|_{t=\tau} = \frac{\Delta P_{imbalance}}{P_{load}} \frac{f_0}{2H} \tag{10}$$

The optimum placement of the renewables can be formulated as an optimization problem. Since the main goal is to study the frequency control response of the power

system, the objective function becomes to minimize the SDF. Mathematically, this is described as follows:

$$\min|SDF| \tag{11}$$

subject to restriction Equations (1) to (8) and the conditions given below,

$$\sum_{n=1}^{N}\left(P_{gen}(n,t) + P_{PV}(t) + P_{WT}(n,t)\right) = \sum_{n=1}^{N} P_{load}(n,t) + \sum_{l=1}^{\ell} P_{losses}(l,t) \tag{12}$$

$$Q_{gen}(t) = \sum_{n=1}^{N} Q_{load}(n,t) + \sum_{l=1}^{\ell} Q_{losses}(l,t) \tag{13}$$

$$|V_{min}| \leq |V_n| \leq |V_{max}| \tag{14}$$

$$0 \leq I_l \leq I_{max} \tag{15}$$

$$N_{PV} \geq 0, \; P_{PV}(t) = P_{PV(peak)} \tag{16}$$

$$N_{WT} \geq 0, \; P_{WT}(t) = P_{wt(peak)} \tag{17}$$

where the restrictions shown in Equations (12) and (13) provide the real and reactive power flow constraints in which the generated real P_{gen} and reactive Q_{gen} by all generators, including renewables (PV system P_{PV} and wind generation P_{WT}), must satisfy the real P_{losses} and reactive Q_{losses} demand at any bus n and time t plus the real and reactive power losses at any branch l and time t. The constraint presented in Equation (14) is designed to keep the voltage within the desired range, while Equation (15) is designed to set the current flow at any branch within the power system. Finally, Equations (16) and (17) are designed to set a certain number of PV systems and wind turbines at any bus, with a power capacity equal to its rate value. This is performed in order to explore the worst scenario, in case renewables are installed.

4. Optimization Algorithm

PSO and GA have proved to be powerful metaheuristic optimization techniques in different areas of science and engineering. For instance, the authors of [28] proposed a combination of artificial neural network and PSO to develop an evolutionary algorithm that minimizes the emissions of CO, HC, and NOx from gasoline blended with hydrogen peroxide and ethanol. In [29], a comprehensive learning particle swarm optimizer (CLPSO) was embedded with local search, and was shown to be more robust in terms of accuracy and convergence rate than traditional PSO. Reference [30] presents a modified genetic algorithm coupled with Monte Carlo method to optimize loading patterns for Pakistan Research Reactor-1. Given the above, this paper focuses on the determination of optimum frequency performance using particle swarm optimization (PSO) [31]. The optimization is performed using Python as the main script, while PowerFactory-DIgSILENT is used to perform and simulate the stability analysis.

The optimization starts by defining the population of particles L at the maximum number of iterations M, which physically represents a set of PV and wind-generation positions at any bus with a specific capacity. Then, a power flow is initiated to obtain information under stationary conditions. Suddenly, an abrupt load disconnection (disturbance) is introduced into the system. Under these conditions, a stability analysis takes place to calculate the SFD index. The position x of the particle ℓ with the best performing (maximum SFD) among the swarm is saved in g, while the best position for each particle is saved in q_ℓ. Then, each particle is given a specific speed $v_\ell(k+1)$ to calculate its new position for the next iteration $x_\ell(k+1)$. The expressions used to calculate v_ℓ and x_ℓ are as follows [31–33]:

$$v_\ell(k+1) = wv_\ell(k) + c_1r_1[q_\ell(k) - x_\ell(k)] + c_2r_2[g(k) - x_\ell(k)] \tag{18}$$

$$x_\ell(k+1) = x_\ell(i) + v_\ell(k+1) \tag{19}$$

where w, c_1, and c_2 are the weights for the inertia whose values are between (0,2), while r_1 and r_2 are random numbers between (0,1). The values used in this article are $\omega = 1.2$, $c_1 = 0.4$, and $c_2 = 0.4$. For more details concerning the algorithm employed, Figure 4 presents a flowchart of the implemented algorithm.
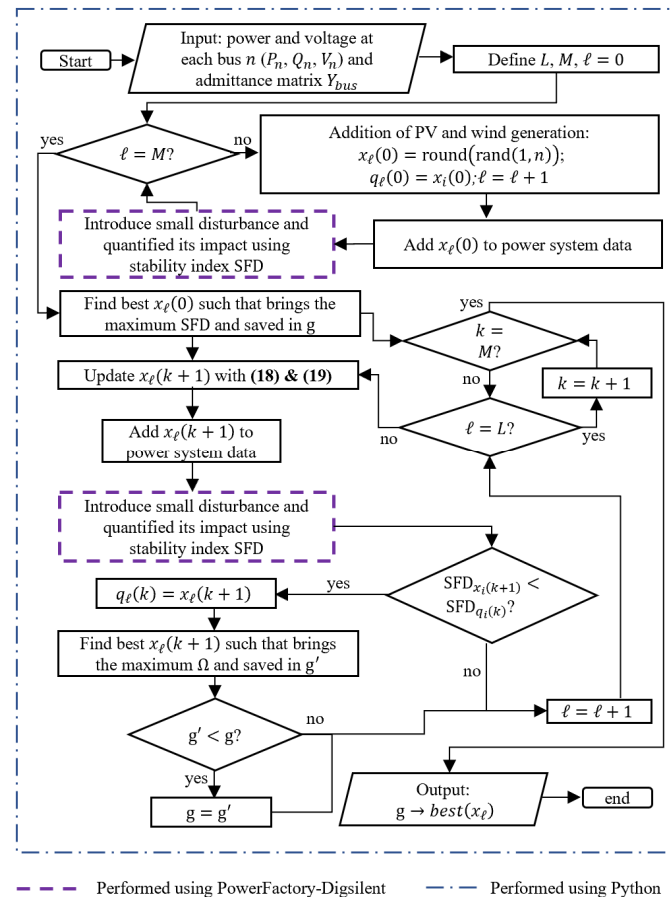

Figure 4. PSO flowchart implemented.

5. Case Study

The power system used to validate the proposed approach is the modified IEEE New England 39-bus test system. The features of the system are specified in [34,35]. It is relevant to mention that the slack bus is equipped with an LFC, AVR, and PSS control using the block diagram as presented in Figures 1–3, respectively. To simplify the analysis, it is assumed that there is enough budget to install a PV system and wind generators of 40 MWp and 100 MWp, respectively. The simulation is executed in Windows 10 Home edition with a processor Intel(R) Core (TM) i7-1065G7 CPU of 1.20–1.50 GHz and a memory RAM of 8.00 GB that runs in a 64-bit operating system.

6. Results and Discussion

The frequency response assessment was performed for three scenarios. The first scenario considered the IEEE 39-bus network without modifications (no RES integrated), and it was used as a benchmark for the other two scenarios. The second scenario incorporated renewable generation in the same buses as conventional generators, i.e., PV and WG connected at buses 2, 5, 6, 10, 19, 23, and 16, creating a total capacity of 1120 MW of renewable installations. The last scenario considered the optimal allocation of the RES as presented in Figure 5, which was obtained using the proposed approach. With a view to showing the impact of the proposed approach, a basic control system was implemented in the RES,

causing pessimistic stability responses in comparison to a comprehensive control system for RES [36]. It is relevant to mention that the disturbance consisted of a suddenly active power imbalance performed through the disconnection of the five highest loads within the system, i.e., load in bus 4, 8, 16, 20, and 39. To perform a representative stability analysis of the power system, the frequency (Figure 6a) and active power (Figure 6b) responses at bus 41 (swing bus) for all scenarios were obtained through PowerFactory-DIgSILENT.
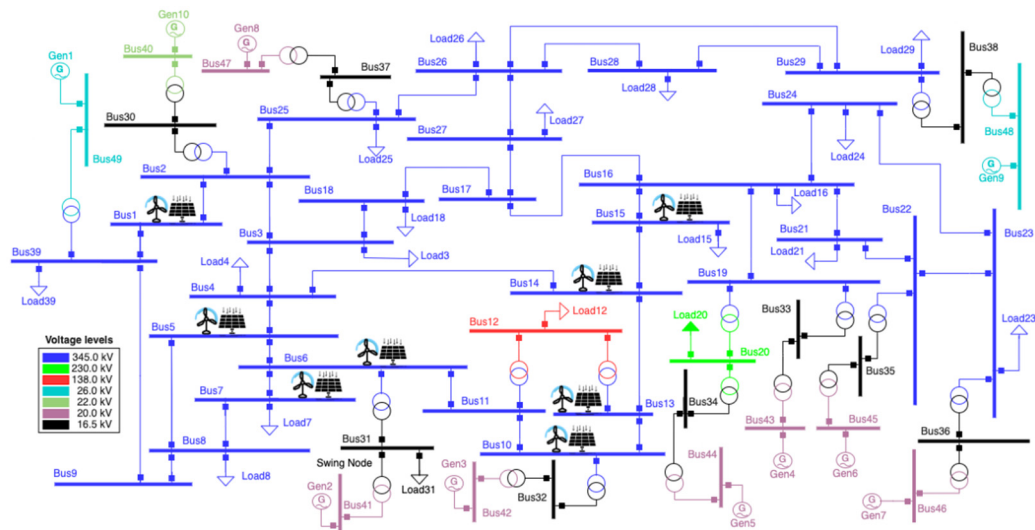

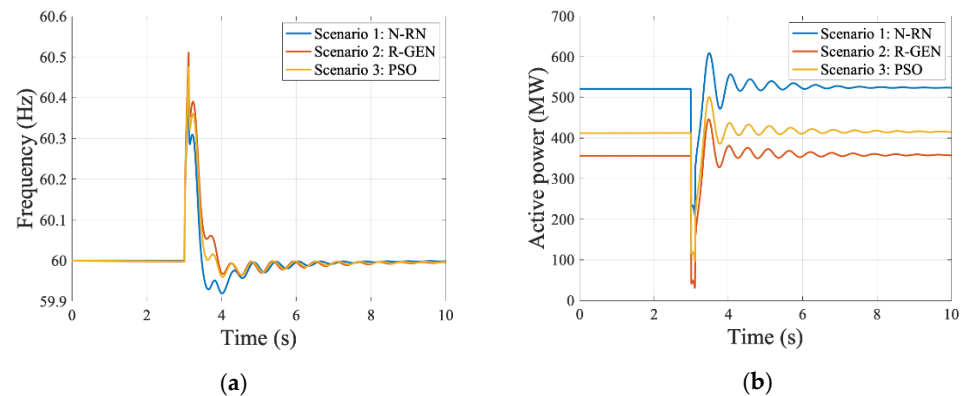**Figure 5.** Optimum allocation of PV and wind generation at IEEE New England 39.

Figure 6. (**a**) Frequency response for slack bus. (**b**) Active power response for slack bus.

Figure 6 reveals that every single case shows a stable response, whereas the frequency transients differ from each other. The stability is reached due to the robustness of the implemented LFC that enables one to control the injection of the active power to compensate imbalances that occur on the frequency response after the disturbance has taken place, resulting in the ROCOF presented in Table 1. Even though the scenario in which renewables are installed (scenarios 2 and 3) presents greater values than the base scenario (no renewables), the scenario with the optimum installation of renewables only differs by around 2% in comparison to the base scenario. Consequently, the installation of renewables negatively affects the transient behavior of the frequency response, but with the optimum installation of renewables, such impact is not considerable.

Table 1. Stability metrics.

| Scenario	SDF	ROCOF	Steady-State Frequency after Perturbance Expressed in Hz
1	1.0034	0.3502	60.3008
2	1.1048	0.3702	60.4445
3	1.0609	0.3562	60.3875

The increasing penetration of renewable energy sources provides new challenges to power system security such as the stochastic nature of the variability of the renewable resources, effects on transient stability, voltage instability, frequency instability, and power quality [37–39]. In response, several authors have proposed methods to add virtual inertia to the power system [40–42] and grid-forming converters [43]; however, these studies do not consider optimal solution at the planning stage. Due to this need, this work implements a new methodology to determine the expansion capability of renewable energies and its impact on the frequency grid response. A measure of frequency response is given by the SDF, which, using the proposed approach, becomes the lowest value at the base (see Table 1). This is attributed to the absence of the RE, i.e., the RE integration with the grid reduces the entire system's inertia, which deteriorates the frequency response [44–46]. However, the optimum placement of the new generation reduces the negative effects related to inertia reduction and the absence of frequency support during the disturbance in comparison with scenario 2. This is possible due to the ability of the PSO to seek to improve the transient frequency response by considering many security restrictions, e.g., voltage constraints (see Figure 7), power flow equations, maximum transfer capacity of the transmission line, and ideal number of RE, which assures the system's stability. Moreover, the validation of the optimal value is presented in Figure 8. This figure shows that the evolution of the SDF value is presented at every iteration, revealing a convergence after iteration 15 with a variance of 6.6049×10^{-5}.
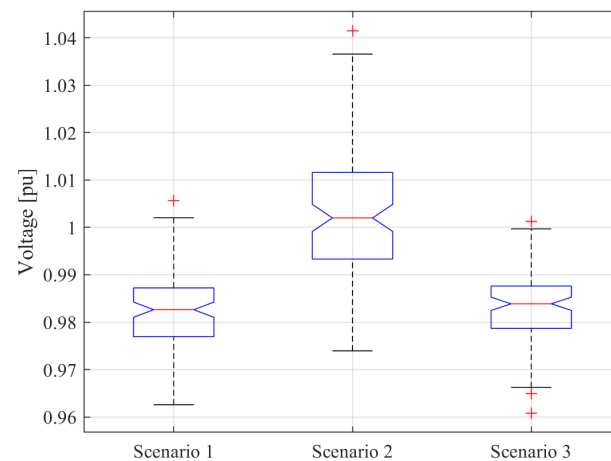
Figure 7. Voltage distribution per scenario.
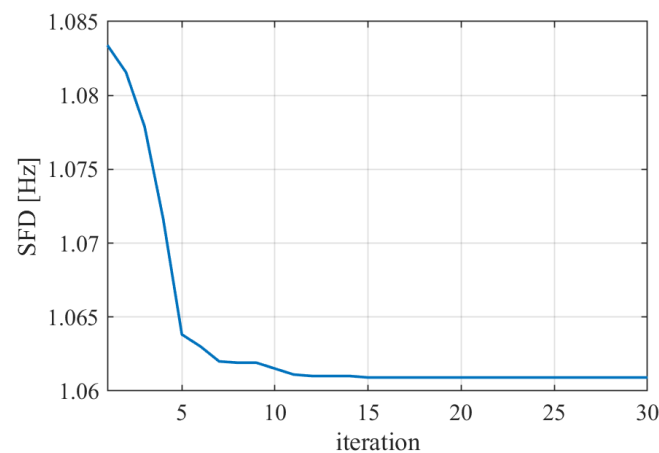
Figure 8. PSO convergence behavior.

To demonstrate an application of the proposed approach, Figure 9 shows the CCT at the base and optimum scenarios, when a three-phase fault occurs at 10% of any line within the power system. The results reveal that the incorporation of the renewables at the optimum allocation leads to a higher time to clear the fault before system collapse in comparison to the base scenario. From the point of view of relay coordination, this is beneficial, as the set point will be able to increase system load to the line without experiencing system instability in case a three-phase fault occurs [47].
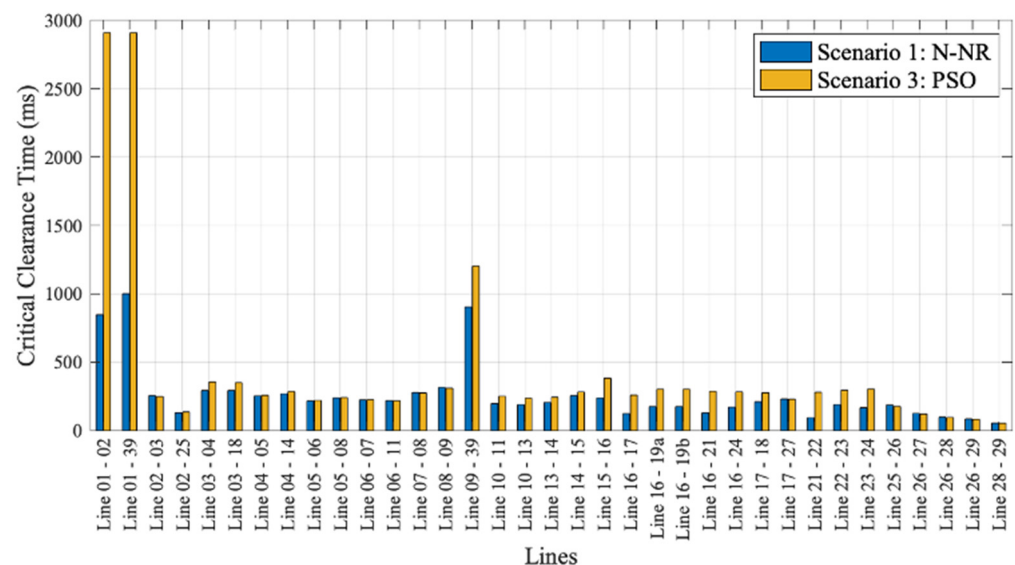
Figure 9. Scenarios 1 and 3 CCT for faults in every line of the network.

7. Conclusions

This paper presents a methodology to determine the capacity of renewable energies that can be integrated into an electrical system, considering a security indicator as an objective function. In particular, the SDF during a severe disturbance in the power system was maximized. The problem includes constraints to guarantee the balance of active and reactive power, line capacity, and nodal voltages. To solve the given problem, a particle swarm optimization algorithm implemented in Python and executed in PowerFactory-DIgSILENT was used to determine the optimal location and size of the renewable generation that reduces the impact of power system disturbance. The results show that the proper allocation of the renewable generation reduces the adverse effects of the perturbation on the transient frequency response, even when the study considered high penetration of wind generation. Future studies are still necessary to further improve the optimization design of

these systems and to perform longer simulations under different scenarios to assure the robustness of this approach. In addition, the implementation of stochastic indices based on sampling techniques (e.g., Monte Carlo simulation, Latin hypercube, etc.) could be explored to measure different operational states of the power system that may drive active contingency planning for the integration of new renewable sources.

References

1. Rodriguez-Gallegos, C.D.; Gandhi, O.; Yang, D.; Alvarez-Alvarado, M.S.; Zhang, W.; Reindl, T.; Panda, S.K. A siting and sizing optimization approach for PV–battery–diesel hybrid systems. *IEEE Trans. Ind. Appl.* **2017**, *54*, 2637–2645. [CrossRef]
2. Recalde, A.A.; Alvarez-Alvarado, M.S. Design optimization for reliability improvement in microgrids with wind–tidal–photovoltaic generation. *Electr. Power Syst. Res.* **2020**, *188*, 106540. [CrossRef]
3. Enslin, J.H.R. Network impacts of high penetration of photovoltaic solar power systems. In Proceedings of the IEEE Power and Energy Society General Meeting, Minneapolis, MI, USA, 25–29 July 2010; pp. 1–5.
4. Babatunde, O.M.; Munda, J.L.; Hamam, Y. Power system flexibility: A review. *Energy Rep.* **2020**, *6*, 101–106. [CrossRef]
5. Lannoye, E.; Flynn, D.; O'Malley, M. Evaluation of power system flexibility. *IEEE Trans. Power Syst.* **2012**, *27*, 922–931. [CrossRef]
6. Alvarez-Alvarado, M.S.; Donaldson, D.L.; Recalde, A.A.; Noriega, H.H.; Khan, Z.A.; Velasquez, W.; Rodriguez-Gallegos, C.D. Power System Reliability and Maintenance Evolution: A Critical Review and Future Perspectives. *IEEE Access* **2022**, *10*, 51922–51950. [CrossRef]
7. Gandhi, O.; Kumar, D.S.; Rodríguez-Gallegos, C.D.; Srinivasan, D. Review of power system impacts at high PV penetration Part I: Factors limiting PV penetration. *Sol. Energy* **2020**, *210*, 181–201. [CrossRef]
8. Kumar, D.S.; Gandhi, O.; Rodríguez-Gallegos, C.D.; Srinivasan, D. Review of power system impacts at high PV penetration Part II: Potential solutions and the way forward. *Sol. Energy* **2020**, *210*, 202–221.
9. Prasad Reddy, P.D.; Veera Reddy, V.C.; Manohar, T.G. Optimal renewable resources placement in distribution networks by combined power loss index and whale optimization algorithms. *J. Electr. Syst. Inf. Technol.* **2018**, *5*, 175–191.
10. Hamida, I.B.; Salah, S.B.; Msahli, F.; Mimouni, M.F. Optimal network reconfiguration and renewable DG integration considering time sequence variation in load and DGs. *Renew. Energy* **2018**, *121*, 66–80. [CrossRef]
11. Min, D.; Ryu, J.; Choi, D.G. Effects of the move towards renewables on the power system reliability and flexibility in South Korea. *Energy Rep.* **2020**, *6*, 406–417. [CrossRef]
12. Rai, A.; Nunn, O. On the impact of increasing penetration of variable renewables on electricity spot price extremes in Australia. *Econ. Anal. Policy* **2020**, *67*, 67–86. [CrossRef] [PubMed]
13. Ehsan, A.; Yang, Q. Optimal integration and planning of renewable distributed generation in the power distribution networks: A review of analytical techniques. *Appl. Energy* **2018**, *210*, 44–59. [CrossRef]
14. Impram, S.; Nese, S.V.; Oral, B. Challenges of renewable energy penetration on power system flexibility: A survey. *Energy Strateg. Rev.* **2020**, *31*, 100539. [CrossRef]
15. Mohandes, B.; El Moursi, M.S.; Hatziargyriou, N.; El Khatib, S. A review of power system flexibility with high penetration of renewables. *IEEE Trans. Power Syst.* **2019**, *34*, 3140–3155. [CrossRef]
16. Sajadi, A.; Strezoski, L.; Strezoski, V.; Prica, M.; Loparo, K.A. Integration of renewable energy systems and challenges for dynamics, control, and automation of electrical power systems. *Wiley Interdiscip. Rev. Energy Environ.* **2019**, *8*, e321. [CrossRef]
17. Shaheen, A.M.; Elsayed, A.M.; El-Sehiemy, R.A.; Abdelaziz, A.Y. Equilibrium optimization algorithm for network reconfiguration and distributed generation allocation in power systems. *Appl. Soft Comput.* **2021**, *98*, 106867. [CrossRef]

18. Aman, M.M.; Jasmon, G.B.; Mokhlis, H.; Bakar, A.H.A. Optimal placement and sizing of a DG based on a new power stability index and line losses. *Int. J. Electr. Power Energy Syst.* **2012**, *43*, 1296–1304. [CrossRef]

19. Kamel, S.; Awad, A.; Abdel-Mawgoud, H.; Jurado, F. Optimal DG allocation for enhancing voltage stability and minimizing power loss using hybrid gray Wolf optimizer. *Turkish J. Electr. Eng. Comput. Sci.* **2019**, *27*, 2947–2961. [CrossRef]

20. Cipriano, D.; Rengifo, J.; Aller, J.M. Transient stability evaluation of high penetration of DFIG controlled by DTC and DPC into power systems. In Proceedings of the 2018 IEEE 3rd Ecuador Technical Chapters Meeting ETCM, Cuenca, Ecuador, 15–19 October 2018; pp. 1–6.

21. Maleki, A.; Askarzadeh, A. Artificial bee swarm optimization for optimum sizing of a stand-alone PV/WT/FC hybrid system considering LPSP concept. *Sol. Energy* **2014**, *107*, 227–235. [CrossRef]

22. Maleki, A.; Askarzadeh, A. Optimal sizing of a PV/wind/diesel system with battery storage for electrification to an off-grid remote region: A case study of Rafsanjan, Iran. *Sustain. Energy Technol. Assess.* **2014**, *7*, 147–153. [CrossRef]

23. Tungadio, D.H.; Sun, Y. Load frequency controllers considering renewable energy integration in power system. *Energy Rep.* **2019**, *5*, 436–453. [CrossRef]

24. Kundur, P. *Power System Stability and Control—Prabha Kundur*; McGraw-Hill Education: New York, NY, USA, 1994; p. 1176.

25. *IEEE Std 421.5-2016*; (Revision of IEEE Std 421.5-2005): IEEE Recommended Practice for Excitation System Models for Power System Stability Studies. IEEE: Piscataway, NJ, USA, 2016; Volume 2016.

26. Eriksson, R.; Modig, N.; Elkington, K. Synthetic inertia versus fast frequency response: A definition. *IET Renew. Power Gener.* **2018**, *12*, 507–514. [CrossRef]

27. Sun, M.; Liu, G.; Popov, M.; Terzija, V.; Azizi, S. Underfrequency load shedding using locally estimated RoCoF of the center of inertia. *IEEE Trans. Power Syst.* **2021**, *36*, 4212–4222. [CrossRef]

28. Barboza, A.B.V.; Mohan, S.; Dinesha, P. On reducing the emissions of CO, HC, and NOx from gasoline blended with hydrogen peroxide and ethanol: Optimization study aided with ANN-PSO. *Environ. Pollut.* **2022**, *310*, 119866. [CrossRef]

29. Cao, Y.; Zhang, H.; Li, W.; Zhou, M.; Zhang, Y.; Chaovalitwongse, W.A. Comprehensive learning particle swarm optimization algorithm with local search for multimodal functions. *IEEE Trans. Evol. Comput.* **2018**, *23*, 718–731. [CrossRef]

30. Shaukat, N.; Ahmad, A.; Mohsin, B.; Khan, R.; Khan, S.U.-D.; Khan, S.U.-D. Multiobjective Core Reloading Pattern Optimization of PARR-1 Using Modified Genetic Algorithm Coupled with Monte Carlo Methods. *Sci. Technol. Nucl. Install.* **2021**, *2021*, 1802492. [CrossRef]

31. Bai, Q. Analysis of Particle Swarm Optimization Algorithm. *Comput. Inf. Sci.* **2010**, *3*, 180. [CrossRef]

32. Alvarez-Alvarado, M.S.; Alban-Chacón, F.E.; Lamilla-Rubio, E.A.; Rodríguez-Gallegos, C.D.; Velásquez, W. Three novel quantum-inspired swarm optimization algorithms using different bounded potential fields. *Sci. Rep.* **2022**, *11*, 11655. [CrossRef]

33. Alvarez-Alvarado, M.S.; Rodríguez-Gallegos, C.D.; Jayaweera, D. Optimal planning and operation of static VAR compensators in a distribution system with non-linear loads. *IET Gener. Transm. Distrib.* **2018**, *12*, 3726–3735. [CrossRef]

34. Athay, T.; Podmore, R. A practical method for the direct analysis of transient stability. *IEEE Trans. Power Appar. Syst.* **1979**, *2*, 573–584. [CrossRef]

35. Pai, M.A. *Energy Function Analysis for Power System Stability*; Kluwer Academic Publishers: Boston, MA, USA, 2012.

36. Elkhidir, L.; Khan, K.; Al-Muhaini, M.; Khalid, M. Enhancing Transient Response and Voltage Stability of Renewable Integrated Microgrids. *Sustainbility* **2022**, *14*, 3710. [CrossRef]

37. Dudurych, I.M. The impact of renewables on operational security: Operating power systems that have extremely high penetrations of nonsynchronous renewable sources. *IEEE Power Energy Mag.* **2021**, *19*, 37–45. [CrossRef]

38. Sperstad, I.B.; Degefa, M.Z.; Kjølle, G. The impact of flexible resources in distribution systems on the security of electricity supply: A literature review. *Electr. Power Syst. Res.* **2020**, *188*, 106532. [CrossRef]

39. Ríos-Ocampo, J.P.; Arango-Aramburo, S.; Larsen, E.R. Renewable energy penetration and energy security in electricity markets. *Int. J. Energy Res.* **2021**, *45*, 17767–17783. [CrossRef]

40. Ding, T.; Zeng, Z.; Qu, M.; Catalão, J.P.S.; Shahidehpour, M. Two-stage chance-constrained stochastic thermal unit commitment for optimal provision of virtual inertia in wind-storage systems. *IEEE Trans. Power Syst.* **2021**, *36*, 3520–3530. [CrossRef]

41. Yang, D.; Jin, E.; You, J.; Hua, L. Dynamic frequency support from a dfig-based wind turbine generator via virtual inertia control. *Appl. Sci.* **2020**, *10*, 3376. [CrossRef]

42. Zhang, X.; Zhu, Z.; Fu, Y.; Li, L. Optimized virtual inertia of wind turbine for rotor angle stability in interconnected power systems. *Electr. Power Syst. Res.* **2020**, *180*, 106157. [CrossRef]

43. Rosso, R.; Wang, X.; Liserre, M.; Lu, X.; Engelken, S. Grid-forming converters: An overview of control approaches and future trends. In Proceedings of the 2020 IEEE Energy Conversion Congress and Exposition (ECCE), Virtual, 11–15 October 2020; pp. 4292–4299.

44. Liu, Y.; Gracia, J.R.; King, T.J.; Liu, Y. Frequency Regulation and Oscillation Damping Contributions of Variable-Speed Wind Generators in the U.S. Eastern Interconnection (EI). *IEEE Trans. Sustain. Energy* **2015**, *6*, 951–958. [CrossRef]

45. Wu, W.; Skye, H.M.; Domanski, P.A. Selecting HVAC systems to achieve comfortable and cost-effective residential net-zero energy buildings. *Appl. Energy* **2018**, *212*, 577–591. [CrossRef]

46. Alam, M.S.; Al-Ismail, F.S.; Salem, A.; Abido, M.A. High-level penetration of renewable energy sources into grid utility: Challenges and solutions. *IEEE Access* **2020**, *8*, 190277–190299. [CrossRef]

47. Carrión, D.; García, E.; Jaramillo, M.; González, J.W. A novel methodology for optimal svc location considering n-1 contingencies and reactive power flows reconfiguration. *Energies* **2021**, *14*, 6652. [CrossRef]